ORIGINAL ARTICLE

Improving VLBI analysis by tropospheric ties in GNSS and VLBI integrated processing

Jungang Wang[1,2,3] · Maorong Ge[1,2] · Susanne Glaser[1] · Kyriakos Balidakis[1] · Robert Heinkelmann[1] · Harald Schuh[1,2]

Abstract

Tropospheric delay modeling is challenging in high-precision Very Long Baseline Interferometry (VLBI) analysis due to the rapid water vapor variation and imperfect observation geometry, where observations from Global Navigation Satellite Systems (GNSS) co-locations can enhance the VLBI analysis. We investigate the impact of tropospheric ties in the VLBI and GNSS integrated processing during the CONT05–CONT17 campaigns, and present a method that automatically handles the systematic tropospheric tie biases. Applying tropospheric ties at VLBI–GNSS co-locations enhances the observation geometry and improves the solution reliability. The VLBI network is stabilized, with station coordinate repeatability improved by 12% horizontally and by 28% vertically, and the network scale improved by 32%. The Earth Orientation Parameters (EOP) improve by up to 20%. Both zenith delay and gradient ties contribute to the improvement of EOP, whereas the gradient ties contribute mainly to the improvement of length of day and celestial pole offsets.

Keywords GNSS · VLBI · Combination on the observation level · Tropospheric tie · Earth orientation parameters

1 Introduction

For the microwave-based space geodetic techniques, such as Very Long Baseline Interferometry (VLBI) and Global Navigation Satellite Systems (GNSS), the signals transmitted through the electrically neutral atmosphere are delayed due to the non-vacuum conditions, causing the tropospheric delay (Böhm and Schuh 2013). Modeling the time-varying tropospheric delay to achieve high-precision space geodesy is challenging due to the rapid spatial and temporal variation of its wet component and the correlation between tropospheric delay and station coordinates and clocks, especially between zenith total delay (ZTD) and the station vertical component. As VLBI is the only technique capable of determining the full

set of Earth Orientation Parameters (EOP) and contributes to the determination of the network scale of the International Terrestrial Reference Frame (ITRF) (Altamimi et al. 2016; Bizouard et al. 2018), persistent efforts have been put to improve VLBI solutions. However, due to the fact that at least two VLBI radio telescopes must observe the same radio source simultaneously, the limited observation number and imperfect observation geometry present disadvantages for VLBI-only studies.

To de-correlate station coordinates and tropospheric parameters, precise external tropospheric information can be used, including water vapor radiometer (Kuehn et al. 1991; Nilsson et al. 2017a, b), Numerical Weather Models (NWMs) (Hobiger et al. 2010; Eriksson et al. 2014; Hofmeister and Böhm 2017), or precise estimates from an independent space geodetic technique, such as GNSS. GNSS provides precise tropospheric information with good temporal resolution and a ZTD accuracy of 4 mm (Bender et al. 2008) due to the continuous tracking and well distributed observation geometry. Thus, it has been widely used to enhance other microwave-based space geodetic techniques, such as satellite altimetry (Fernandes et al. 2015) and Interferometric Synthetic Aperture Radar (InSAR) (Williams et al.

✉ Jungang Wang
  jgwang@gfz-potsdam.de

1 GFZ German Research Centre for Geosciences, Telegrafenberg, 14473 Potsdam, Germany

2 Institut für Geodäsie und Geoinformationstechnik, Technische Universität Berlin, Kaiserin-Augusta-Allee 104-106, 10553 Berlin, Germany

3 Shanghai Astronomical Observatory, Chinese Academy of Sciences, 80 Nandan Road, Shanghai 200030, China

1998; Shamshiri et al. 2020). At co-location sites that typically extend hundreds of meters, VLBI and GNSS can be assumed observing through the same troposphere. Thus, the tropospheric zenith delays and horizontal gradients can be combined after considering the effects of station coordinate differences on tropospheric parameters, that is, the tropospheric ties. Applying tropospheric ties allows to consider more observations and improves the observation geometry, leading to a better precision of tropospheric parameters. Through inter-parameter correlations, other parameters can be improved in turn, including station positions and EOP, especially those of the VLBI solution that suffer more from the limited geometry.

Applying tropospheric ties to GNSS co-locations can improve the UT1-UTC (dUT1) accuracy of the International VLBI Service for Geodesy and Astrometry (IVS) 1-h Intensive sessions to overcome the deficiency of poor geometry (Teke et al. 2015; Nilsson, et al. 2017a, b). The IVS 24-h sessions also benefit from tropospheric ties to GNSS co-locations (Krügel et al. 2007; Hobiger and Otsubo 2014; Diamantidis et al. 2021), where station coordinates improve. However, most of these studies use different software for the VLBI and GNSS processing. Despite the great efforts in pursuing homogeneous processing strategies, the inter-software inconsistency inevitably causes tropospheric delay discrepancy and degrades the solution. More importantly, the tropospheric tie might present systematic biases even after applying the height-related corrections, which can reach up to 5 mm for ZTD. Ignoring them may distort the VLBI network and cause systematic biases in the VLBI estimates. Moreover, these studies mainly focus on the station coordinates, whereas the impact on global geodetic and geophysical parameters, including the network scale and EOP, has not been fully investigated.

The current ITRF determination by combining different space geodetic techniques utilizes the global ties, that is, EOP, and local ties on station coordinates at co-location sites as well as co-motion constraints. Additionally applying tropospheric ties will very likely be an important step forward in ITRF determination. Considering the high number of parameters, combining tropospheric parameters has a large potential to improve the precision and reliability, and to contribute to validating the local ties (Krügel et al. 2007). The combination on the observation level can also improve the consistency and reliability of the future determination of reference frames and EOP.

In this study, we investigate the impact of applying tropospheric ties at VLBI–GNSS co-location sites based on the five IVS Continuous VLBI Campaigns (CONT) between 2005 and 2017. We process the VLBI and GNSS observations simultaneously in the same software package, that is, integrated processing on the observation level, to ensure the highest consistency. Furthermore, we adopt an automatic

method to handle the tropospheric tie biases. We demonstrate the effects of ZTD and gradient ties on station coordinates, network scale, and EOP individually.

2 Data and methods

2.1 The VLBI CONT campaigns

Unlike GNSS where daily observations are usually processed in the 00:00–24:00 UT datasets, the 24-h global VLBI observing sessions are usually discontinuous and start around 17:00–18:30 UT. However, the 24-h sessions available in the five CONT campaigns start at 00:00 UT, named with the year carried out as CONT05, CONT08, CONT11, CONT14, and CONT17, with 15 sessions in each campaign. It should be noted that the CONT05 sessions started observing at 17:00, but a reprocessed version (the XB series) starting at 00:00 is also provided by IVS and used in this study. The CONT05B series has 14 instead of 15 sessions. The CONT campaigns using more radio telescopes and radio sources aim on demonstrating the best capability of VLBI at that time on both technical and scientific perspectives (Behrend et al. 2020). Therefore, they are ideal for inter-technique comparisons and multi-technique combinations (Thaller et al. 2006; Teke et al. 2013; Hobiger and Otsubo 2014; Pollet et al. 2014; Heinkelmann et al. 2016). The geographical distribution of the network stations of the CONT05–CONT17 campaigns used in this study is presented in Fig. 1.

Figure 1 also shows the co-locations with the International GNSS Service (IGS) stations, which are available at most VLBI stations. We use all available GNSS co-locations to improve the observation geometry and to alleviate potential instrument-related systematic biases.

The GNSS–VLBI inter-station distances are provided in Table 1. For most of the co-locations, the horizontal distances are within 200 m, and the vertical distances are within 20 m. The two exceptions are: MDO1–FD-VLBA, 8 km horizontally and around 400 m vertically; HAR-B–HART15M/HARTRAO, 2 km horizontally and around 150 m vertically. Despite this relatively large inter-station distance, the inter-technique agreement of tropospheric parameters at these two co-locations is not larger than that of other co-locations. For MDO1–FD-VLBA, the STD value of ZTD differences in CONT17-VLBA is 4.1 mm, and the RMS values of the north and east gradient differences are 0.6 and 0.4 mm, respectively. As for HAR-B–HART15M/HARTRAO, the STD value of ZTD differences varies between 3.8 and 6.8 mm, and the RMS value of north and east gradients varies between 0.5 and 1.6 mm, during CONT05 to CONT17. For all the co-locations during CONT05 and CONT17, the average value is 4.0 mm for ZTD STD, 0.7 mm for north gradient, and 0.6 mm for
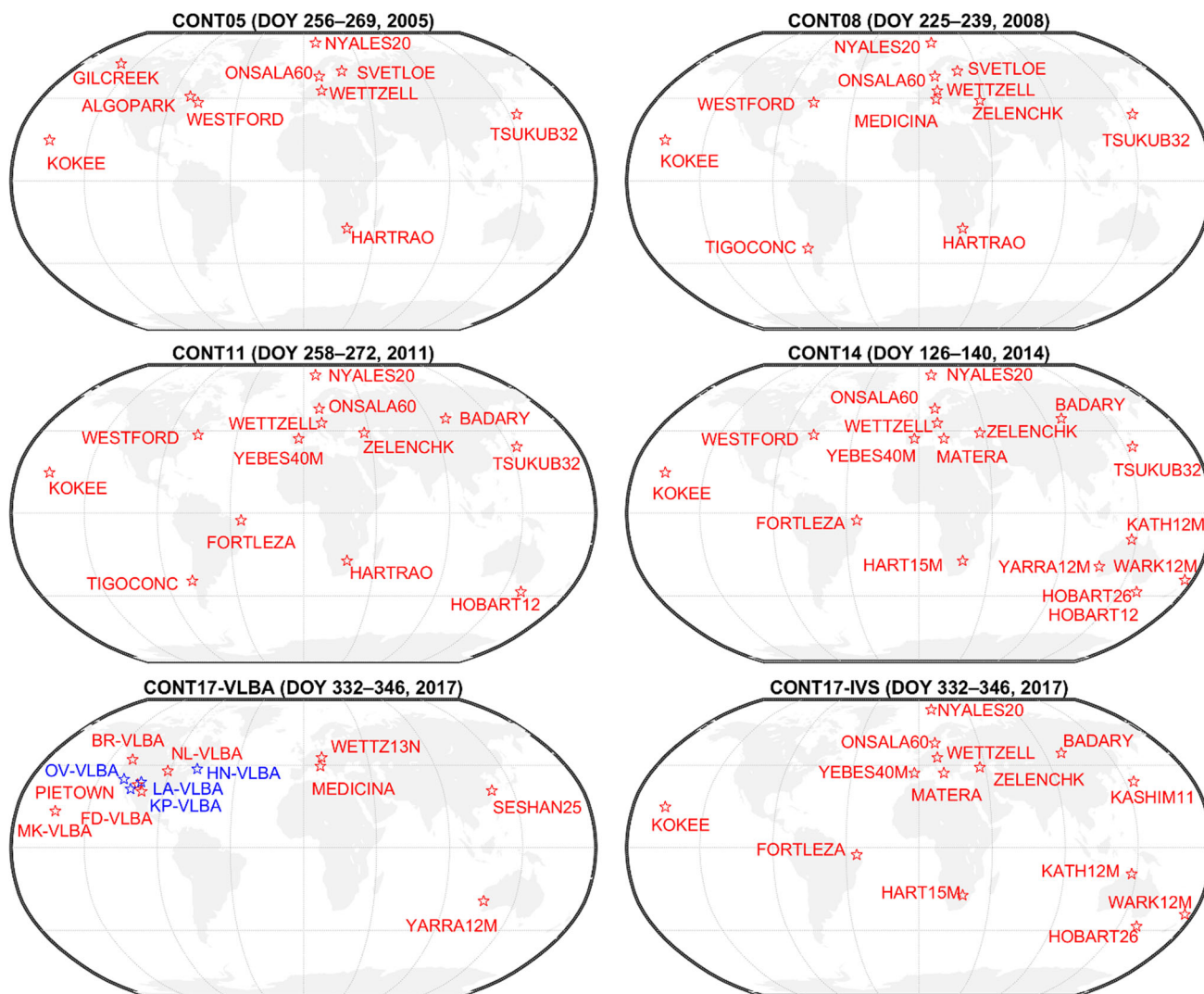
Fig. 1 Distribution of VLBI stations in CONT05–CONT17. Red are stations with and blue without GNSS co-location. In CONT17 the VLBA and IVS legacy networks observed in parallel. The start and end times of each campaign are given in terms of Day Of Year (DOY) in the title of each panel

east gradient. Therefore, the tropospheric ties at MDO1–FD-VLBA and HARB–HART15M/HARTRAO co-locations can be applied.

2.2 Integrated processing of GNSS and VLBI on the observation level

For the multi-technique integrated processing on the observation level, the VLBI module was newly implemented in the Positioning And Navigation Data Analyst (PANDA) software (Liu and Ge 2003). The PANDA software focusing on high-precision GNSS data processing is widely used in geodetic applications, including satellite orbit determination (Liu et al. 2016; Huang et al. 2020), static and kinematic platform positioning (Penna et al. 2018; Wang and Liu 2019; Abbaszadeh et al. 2020), atmospheric sensing (Wang et al.

2019; Wu et al. 2020). The VLBI module was implemented in a common least-squares estimator with GNSS (Wang 2021), following the IERS Conventions 2010 (Petit and Luzum 2010).

We processed VLBI and GNSS observations simultaneously on a daily basis. The data processing strategy is present in Table 2. The a priori EOP were derived from the IERS Bulletin A product, and the station displacements include solid Earth tides, ocean tidal displacements, pole tide loading, ocean pole tide loading, and tidal atmospheric pressure loading. Non-tidal atmospheric pressure loading (Männel et al. 2019) was also applied using the VMF product (Wijaya et al. 2013).

We processed VLBI X-band group delay observations that were corrected for dispersive delays employing the S-band observations for mitigating the ionospheric refraction. We

Table 1 Inter-station distance of GNSS–VLBI co-locations used in this study. For GNSS stations, the distance between marker and antenna reference point is considered

VLBI	GNSS	North [m]	East [m]	Up [m]
ALGOPARK	ALGO	33.5	105.3	− 23.2
BADARY	BADG	− 61.9	73.5	− 10.2
BR-VLBA	BREW	33.3	48.0	− 11.9
FD-VLBA	MDO1	5046.0	− 6726.0	392.5
FORTLEZA	BRFT	45.5	35.7	− 1.4
GILCREEK	FAIR	− 45.9	− 81.4	− 13.0
HART15M	HARB	307.2	2303.2	151.7
	HRAO	− 40.8	271.9	4.8
HARTRAO	HARB	308.7	2190.3	144.2
	HRAO	− 39.3	159.0	− 1.6
HOBART12	HOB2	95.9	48.7	0.1
HOBART26	HOB2	− 125.6	− 146.0	− 24.0
KASHIM11	KSMV	− 24.1	18.3	− 4.7
KATH12M	KAT1	− 59.4	97.2	− 5.0
KOKEE	KOKB	− 41.8	18.0	− 9.1
	KOKV	− 41.8	18.0	− 9.1
MATERA	MAT1	− 51.4	44.7	− 8.8
	MATE	− 43.7	37.3	− 7.6
MEDICINA	MEDI	− 59.6	− 9.6	− 17.1
MK-VLBA	MKEA	− 3.3	− 87.3	− 8.4
NL-VLBA	NLIB	18.5	− 62.9	− 15.2
NYALES20	NYA1	49.5	− 94.1	− 3.1
	NYA2	136.3	− 237.2	− 5.9
	NYAL	52.9	− 98.8	78.5
ONSALA60	ONS1	− 56.0	− 109.0	− 14.8
	ONSA	− 60.0	− 50.5	− 12.7
PIETOWN	PIE1	54.3	24.3	− 17.1
SESHAN25	SHAO	53.3	74.7	− 7.4
SVETLOE	SVTL	57.6	− 58.5	− 9.3
TIGOCONC	CONT	− 13.6	− 20.8	2.5
	CONZ	− 115.9	− 30.0	9.7
TSUKUB32	TSK2	269.7	− 145.9	− 14.8
	TSKB	281.2	− 111.6	− 17.5
WARK12M	WARK	44.3	− 42.6	− 16.6
WESTFORD	WES2	43.0	38.4	− 1.7
WETTZELL	WTZA	− 87.1	105.8	− 3.1
	WTZR	− 90.1	106.3	− 3.0
	WTZS	− 24.7	85.8	− 5.6
	WTZZ	− 88.6	105.9	− 2.9
WETTZ13N	WTZA	34.8	87.7	− 6.6
	WTZR	31.8	88.2	− 6.5
	WTZS	97.3	67.6	− 9.1
	WTZZ	33.3	87.8	− 6.4

Table 1 (continued)

VLBI	GNSS	North [m]	East [m]	Up [m]
YARRA12M	YAR2	65.9	131.8	− 6.8
	YAR3	72.4	148.7	− 5.8
	YARR	62.0	131.5	− 6.9
YEBES40M	YEBE	26.0	− 149.7	− 16.2
ZELENCHK	ZECK	64.8	− 7.9	− 8.8

estimated daily constant station coordinates applying minimum datum constraints (Glaser et al. 2015) to ITRF2014 (Altamimi et al. 2016). The radio source coordinates were fixed to ICRF3 (Charlot et al. 2020). Both, offsets and rates of polar motion (PM) and UT1-UTC were estimated, whereas celestial pole offsets (CPO, dX and dY) were determined as daily constants. We used the random walk process to model station clocks with a stochastic noise of 0.3 mm/$\sqrt{s}$, and clock breaks and baseline clock offsets where indicated.

We processed the GNSS ionosphere-free combined pseudo-range and phase observations in the static Precise Point Positioning (PPP) mode (Zumberge et al. 1997), with satellite orbits and clocks fixed to IGS products (Johnston et al. 2017; Griffiths 2018). We estimated GNSS receiver clocks as epoch-wise white noise, and corrected antenna phase center offsets and variations (Rebischung and Schmid 2016), phase wind up (Wu et al. 1993), and relativity effect. Note that in PPP mode GNSS observations do not contribute to the EOP estimation.

2.3 Applying the tropospheric ties

For both VLBI and GNSS, the tropospheric delay $L(e, \alpha)$ in slant direction with elevation e and azimuth α can be described as

$$L(e, \alpha) = mf_h(e) \cdot \text{ZHD} + mf_w(e) \cdot (\text{ZWD}_0 + \Delta\text{ZWD})$$
$$+ mf_g(e) \cdot (\cos(\alpha) \cdot G_N + \sin(\alpha) \cdot G_E)$$

$$(1)$$

where ZHD and ZWD_0 denote the a priori zenith hydrostatic and wet delays, respectively; $mf_h(e)$ and $mf_w(e)$ are corresponding mapping functions. G_N and G_E are the north and east total gradients, respectively, and $mf_g(e)$ is the gradient mapping function. The residual non-hydrostatic delay ΔZWD is parametrized as one-hourly piece-wise-constant (PWC), and both gradients are estimated as three-hourly PWC.

The same tropospheric parameters, that is, the residual ZWD and gradients, were applied to both VLBI and GNSS

Table 2 Strategy for VLBI and GNSS integrated processing used in this study

Item	VLBI	GNSS
Mode	Single-session solution	Daily Precise Point Positioning (PPP)
Period	CONT05–CONT17	Same as VLBI
Station	Most of the participating stations	Selected IGS stations co-located with the VLBI stations
Observable	All X-band group delays with the quality code "0"	Un-differenced ionosphere-free linear combination of GPS L1 and L2 phase and pseudo-range observations
Weighting	Constant (1 cm) + observation noise + ionospheric delay noise	0.01 m for LC, 0.9 m for PC; elevation-dependent down-weighting for elevation below 30°:$1/(2 \sin e)$
Cut-off elevation	No	5°
Space part	Radio source coordinates fixed to ICRF3	Satellite orbits and clocks fixed to the IGS 2nd reprocessing product
A priori TRF	ITRF2014 (Altamimi et al. 2016) with velocity and PSD correction	IGS14 with velocity and PSD correction
Site position	No-net-rotation (NNR) and no-net-translation (NNT) for the stations defined in ITRF2014	Estimated as daily constant without constraints
Receiver clock	Linear function plus random walk noise of 0.3 mm/$\sqrt{s}$	Epoch-wise white noise
Ionospheric delay	First order correction from NGS, no higher-order considered	First order corrected by ionosphere-free combination, no higher-order considered
Antenna offset, etc.	Radio telescope eccentricity from ECCDAT.ecc, thermal deformation and axis offset corrected	Receiver and satellite PCV and PCO corrected using IGS14.atx
EOP estimation	PM and UT1-UTC: daily offset and rate, CPO: daily offset	No
Tropospheric delay modeling	A priori value from the 6-hourly sampled VMF3-site and VMF3-grid (1° × 1°) product, temporally linear interpolated, and spatially bilinear interpolated. The a priori gradient value is not applied. Residual Zenith Wet Delay (ZWD) estimated as 1-h piece-wise-constant (PWC); north and east gradients estimated as 3-hourly PWC. Gradient mapping function: Chen and Herring (1997)	
Ephemeris	JPL DE405	
Station displacement	IERS 2010 Conventions (Petit and Luzum, 2010) adopted for: solid Earth tides, ocean tides, pole tide, ocean pole tide, S1-S2 atmospheric pressure loading. Non-tidal atmospheric pressure loading from the VMF product	
EOP modeling	A priori value from the IERS Bulletin A product; sub-daily model follows the IERS 2010 Conventions	

stations at the co-locations, considering the topography-related (mainly in the altitude component) and instrument-related differences. We used the VMF3 station-based product (Landskron and Böhm 2017, 2018) for the a priori zenith delays and mapping functions, which can efficiently cancel the topography-related difference. As the station-based VMF3 does not always refer to the height of the reference point of the GNSS antenna, an empirical equation was applied to correct for this difference (Kouba 2007).

Besides the topography-related tropospheric delay differences, systematic biases are also observed in VLBI–GNSS tropospheric parameter comparisons. For instance, at Westford (WESTFORD–WES2) a 4–5 mm bias has been reported (Steigenberger et al. 2007; Teke et al. 2011), probably due

Table 3 The different solutions with different tropospheric tie setups

Solution	ZTD ties	Gradient ties
NO	No	No
ZTD	Yes	No
GRD	No	Yes
TRP	Yes	Yes

to the GNSS instrument effect. As ignoring this bias might cause network distortion and potentially degrades the solution, we set up a daily constant tropospheric tie bias parameter Δx as

$$x_{\text{GNSS}} = x_{\text{VLBI}} + \Delta x \tag{2}$$

where x_{GNSS} and x_{VLBI} are tropospheric parameters (residual ZWD and gradients) of GNSS and VLBI, respectively. Δx is constrained to the a priori value:

$$\Delta x = \Delta x_{\text{apriori}} \pm \sigma \tag{3}$$

where σ is the uncertainty and adjusted automatically until the normalized residual is less than 1.96 (Baarda, 1968; Lehmann 2012). Since the topography-related bias has already been accounted for, the variable a priori should be zero in case of no instrument-related effects. However, it is usually not the case in reality and the reason is still under investigation. At each VLBI–GNSS co-location, the average tropospheric parameter difference from the single-technique analysis in each campaign was used as the a priori value. Despite the effort to provide precise a priori tropospheric tie bias determined from single-technique solutions, it is still necessary to allow the tropospheric tie bias to vary a bit instead of fixing to the a priori value in the integrated processing. The reason is that currently the tropospheric parameter agreement between GNSS and VLBI is at the level of 4–6 mm (Teke et al. 2013), and the precision of tropospheric tie bias from single-technique solution is not good enough for the tightly fixed solution. We thus propose the automatic weighting strategy to handle tropospheric tie biases, which can be implemented in the long-term multi-technique integrated processing. In future studies, the best way to handle tropospheric tie bias would be carefully calibrating the values and directly applying the values cautiously in integrated processing.

To investigate the different impact of ZTD and gradient ties, four different setups are performed and shown in Table 3. Note that in solution "TRP" the full set of tropospheric ties, including both ZTD and gradients, are applied. At each co-location, the tropospheric ties are applied at all VLBI–GNSS pairs but not at GNSS–GNSS or VLBI–VLBI

pairs to improve the VLBI solution and not over-weight the GNSS solution. In all four solutions GNSS and VLBI observations were processed simultaneously in the common least-squares estimator.

3 Results and discussions

3.1 VLBI station coordinates and network scale

The repeatabilities of station coordinates and network scale indicate the capability to reproduce the terrestrial reference frame using the same network and data processing strategy, and can be used to demonstrate the solution precision and stability. The repeatability is calculated as the weighted standard deviation (WSTD):

$$\begin{aligned}
\text{WSTD} &= \sqrt{\frac{\sum_{i=1}^{n} \frac{(X_i - X_{\text{WMEAN}})^2}{\sigma_i^2}}{\sum_{i=1}^{n} \frac{1}{\sigma_i^2}}} \\
X_{\text{WMEAN}} &= \frac{\sum_{i=1}^{n} \frac{X_i}{\sigma_i^2}}{\sum_{i=1}^{n} \frac{1}{\sigma_i^2}} \\
\text{WRMS} &= \sqrt{\frac{\sum_{i=1}^{n} \frac{X_i^2}{\sigma_i^2}}{\sum_{i=1}^{n} \frac{1}{\sigma_i^2}}}
\end{aligned} \tag{4}$$

where X_i is the estimate at epoch i of all the n solutions and σ_i is the corresponding formal error. The weighted root mean square (WRMS) statistic is further used in Sect. 3.2.

As the tropospheric parameters have a strong correlation with station coordinates, applying tropospheric ties will strengthen the tropospheric parameters and decrease the correlation, and consequently improve the station coordinates, especially in the height component, and subsequently the network scale. The repeatabilities of all station coordinates and the network scale are given in Fig. 2 for each campaign. The network scale is calculated by the seven-parameter Helmert transformation between daily adjusted and a priori coordinates from ITRF2014.

Applying tropospheric ties (solution "TRP") improves the horizontal components in almost all campaigns. The average repeatability is reduced from 2.6 to 2.3 mm and from 2.4 to 2.1 mm in the north and east components, respectively, that is, 12% improvement compared to the solution without tropospheric ties (solution "NO"). When applying only ZTD or gradient ties improves the repeatability in general, the repeatability is slightly degraded (by 0.1 mm) in a few campaigns, for instance, in CONT17. The horizontal improvement from gradient ties is attributed to the

Fig. 2 Repeatability of VLBI north, east, and up coordinate components and network scale. The four solutions are: no tropospheric ties applied ("NO") in red; only ZTD ties applied ("ZTD") in green; only gradient ties applied ("GRD") in blue; both ZTD and gradient ties applied ("TRP") in black. The average values over CONT05–CONT17 are given in brackets, as well as the improvement of solutions with tropospheric ties compared to that without tropospheric ties
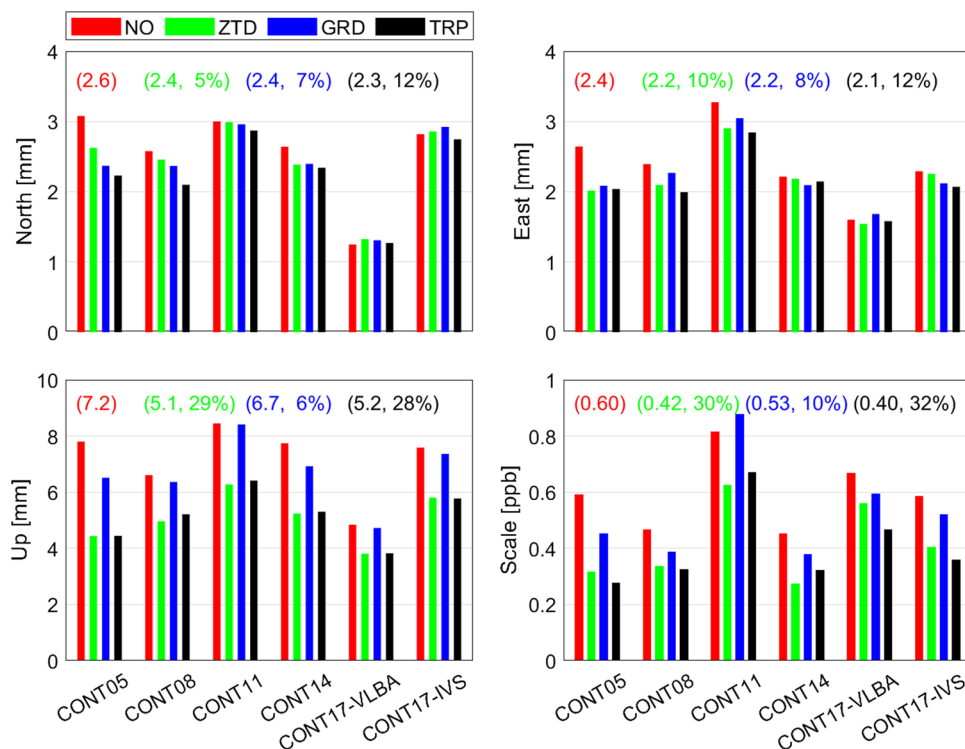
decorrelation between tropospheric gradients and horizontal coordinate components.

Applying tropospheric ties improves the average repeatability of the vertical component over all campaigns by 28% compared to the solution without tropospheric ties, with the value reduced from 7.2 to 5.2 mm, which can be mainly attributed to the ZTD ties, as applying ZTD ties to the precise GNSS estimates alleviates the correlation between the vertical coordinate and ZTD. The repeatability of solutions with only ZTD ties (solution "ZTD") and that with only gradient ties (solution "GRD") is 5.1 and 6.7 mm, respectively, corresponding to an improvement of 29 and 6%. Moreover, all campaigns show consistent improvement.

The VLBI network scale is improved by 32% with the repeatability reduced from 0.60 ppb (solution "NO") to 0.40 ppb (solution "TRP"). The repeatability of solution "ZTD" (0.42 ppb) is better than that of "GRD" (0.53 ppb). Moreover, the solution "ZTD" always has better repeatability in different campaigns, whereas the solution "GRD" ties has worse repeatability in CONT11 (by 0.06 ppb). As the network scale is mainly determined by the station vertical coordinate, the scale improvement is attributed to the ZTD ties.

The station-wise coordinate repeatability differences between solution "NO" without tropospheric ties and solution "TRP" with both ZTD and gradient ties are given in Fig. 3. We can see that most of the VLBI stations have reduced coordinate repeatability values when the tropospheric ties are applied, and as expected the Up component has the largest improvement, which is consistent with the above analysis. In each campaign, a relatively large improvement is usually observed at the VLBI stations with weaker observation geometry. Taking CONT05 as an example, both ALGOPARK and HARTRAO have larger improvement than other stations, and their repeatability values of the solution "NO" are 12.9 and 10.3 mm, respectively, mainly due to the weaker observation geometry: HARTRAO is located in the Southern Hemisphere with around 600 observations per session and ALGOPARK has around 600 observations per session, whereas the rest stations have about 1000–1600 observations per session. The same conclusion applies to other campaigns, such as TIGOCONC in CONT08 (only around 500 observations per session compared to 1000–2400 observations at other stations), ZELENCHK in CONT11 and CONT14 (worse observation quality), and SESHAN25 and YARRA12M in CONT17-VLBA (far from other stations). Among the six networks, the CONT17-VLBA shows the least improvement, with the majority of stations located in North America showing almost no improvement. A few VLBI stations show deteriorated precision up to 1 mm, including the up component of TSUKUBA in CONT08, the north component of TIGOCONC in CONT11, and the east component of FORTLEZA in CONT14. The possible reason is that the observation geometry between co-located GNSS and VLBI stations are different as these VLBI stations are more far

Fig. 3 VLBI station coordinate repeatability differences between solution "NO" without tropospheric ties and solution "TRP" with both ZTD and gradient ties in CONT05–CONT17. The negative value means that the solution "TRP" has improved precision with smaller repeatability
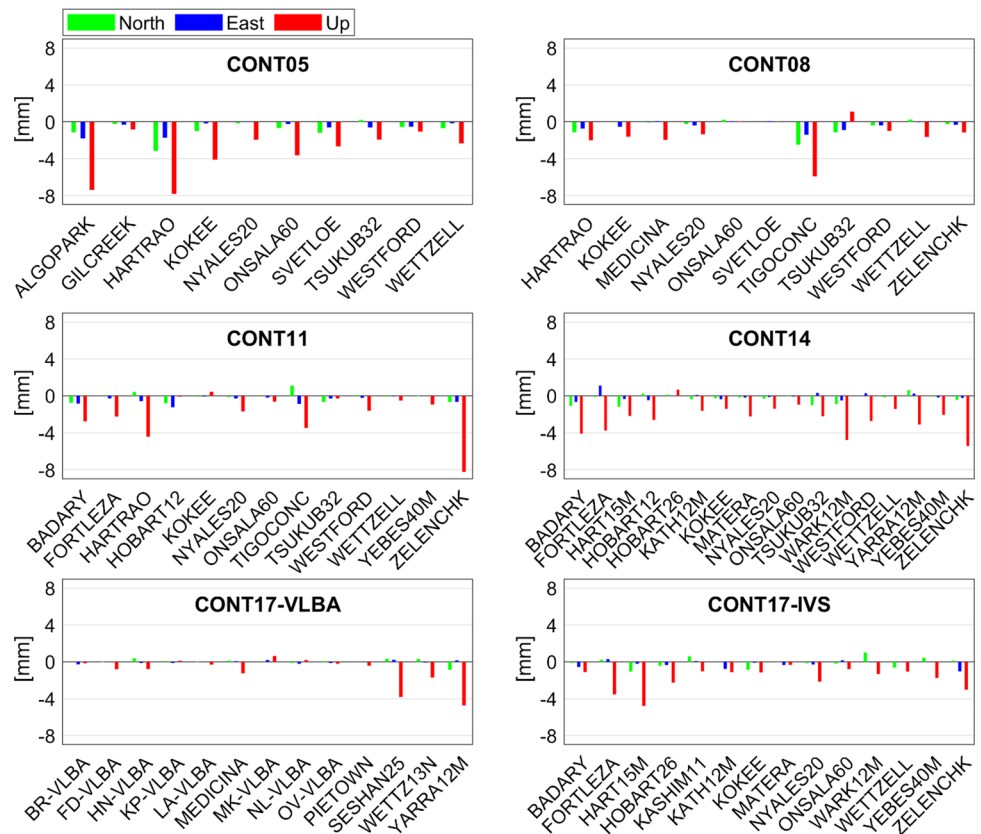
away from other stations, and the local weather condition might have rapid fluctuation.

In addition to the repeatability of the station coordinate and network scale, the VLBI baseline length repeatability is also investigated. The baseline length repeatability is not affected by the global parameters such as EOP or the datum constraints, and thus can better indicate the internal precision of the VLBI solution. Figure 4 gives the VLBI baseline length repeatability values of different solutions. Applying tropospheric ties improves the VLBI baseline length repeatability by 1.7 mm on average, and the contribution of ZTD ties is more significant than that of the gradient ties. Moreover, the longer baselines show larger improvement, which is expectable as the major improvement comes from ZTD ties in the up component.

In addition to the significant improvement on the VLBI TRF, the GNSS station coordinates average repeatability is also improved by 2% horizontally and 6% vertically. This relatively small improvement is because GNSS provides better observation geometry with always enough satellites tracked every epoch. The GNSS average repeatability is 1.7, 2.5, and around 4 mm in north, east, and up components, respectively.

3.2 Earth orientation parameters

We evaluate the EOP precision by comparing to the IERS EOP 14 C04 product (Bizouard et al. 2018), and the polar motion and UT1-UTC precision by the day-boundary-discontinuity (DBD, the misclosure at midnight). The IERS EOP 14 C04 is considered to be of high quality as a multi-technique multi-solution combination product (Glaser et al. 2020), whereas the DBD indicates the internal precision. The WSTD of the EOP differences and WRMS of DBD calculated using Eq. 4 are shown in Fig. 5. We can see that applying tropospheric ties improves VLBI EOP estimates in general, as both the agreement to the IERS product and the DBD statistics are improved on all EOP components on average.

The average WSTD values without tropospheric ties are 97 and 78 μas for the x-pole and y-pole offsets, respectively. Applying only ZTD ties reduces the WSTD values by 21% to 77 μas for x-pole and by 11% to 69 μas for y-pole; and the corresponding improvements by applying only gradient ties are 4% (to 93 μas) and 2% (to 76 μas). Applying tropospheric ties (solution "TRP" compared to "NO") improves the x-pole offset by 18% and the y-pole offset by 13%. The average improvements of PM rates by ZTD ties are 7% for the x-pole rate and 3% for the y-pole rate, and the corresponding improvements by gradient ties are 11 and 14%. Compared to the solution "NO", the average WSTD values of solution

Fig. 4 Left: VLBI weighted baseline length repeatability (WBLR) and the fitting results with different tropospheric ties applied. Right: VLBI WBLR differences of solutions with different tropospheric ties applied with respect to the reference solution (solution "NO" with no ties applied); the mean and median values of the improvement are given in the brackets; a negative value means improvement
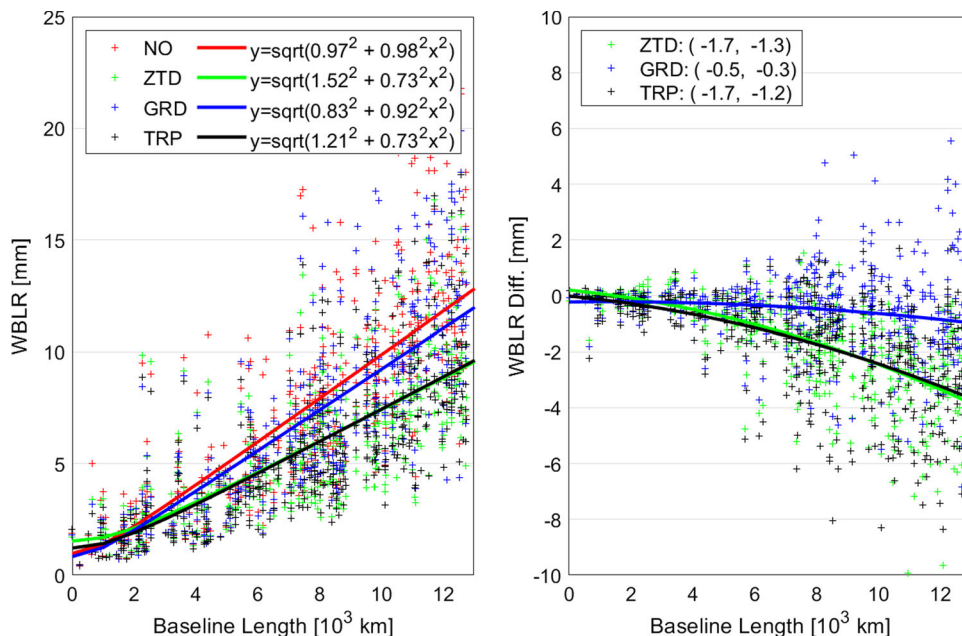
"TRP" are reduced by 12% for x-pole rate and 14% for y-pole rate. The PM DBD is further improved by ZTD ties, and the average improvements by tropospheric ties (solution "TRP" compared to "NO") are 5 and 10% for the x-pole and y-pole components, respectively. For the PM rates, the contribution of gradient ties is larger than that of ZTD ties.

The impact of applying tropospheric ties (solution "TRP" compared to solution "NO") on UT1-UTC is not significant (average improvement of 2%), and results of different campaigns are not conclusive. The Length of Day (LoD, the negative first time derivative of dUT1) WSTD is reduced from 17.2 (solution "NO") to 15.6 μs/day by gradient ties (solution "GRD"), and further to 15.4 μs/day (10% improvement) by additional ZTD ties (solution "TRP"). The UT1-UTC DBD is reduced from 10.5 μs in solution "NO" to 8.7 μs in solution "TRP" (17% improvement), and the major contribution comes from the gradient ties (12% improvement). Both UT1-UTC DBD and LoD statistics are improved by applying tropospheric ties in all CONT campaigns.

The impact of the tropospheric ties on CPO (dX and dY) is diverse in different campaigns. Compared to the solution "NO" without ties, the WSTD values in solution "TRP" are reduced from 48 to 42 μas and from 49 to 47 μas on the dX and dY components, respectively, corresponding to an improvement of 13% and 4%.

The IERS EOP 14 C04 product is not independent as it also uses the data of the CONT campaigns, especially the UT1-UTC and CPO which are more dominated by the VLBI observations of these CONT campaigns (Bizouard et al. 2018). We thus compared the ERP estimates of VLBI solutions to those of the GNSS precise orbit determination (POD) solutions. The GNSS POD solution is performed in

the same time period of the CONT campaigns, adopting a similar processing strategy presented in Table 2. However, in the POD solution (1) more than 200 globally distributed IGS stations are processed; (2) the Earth Rotation Parameters (ERP, including polar motion and LoD) are estimated, including offset and rate for polar motion and rate for UT1-UTC, that is, LoD; (3) the dynamic satellite orbits are estimated; and (4) the GNSS ground station coordinates are estimated with the minimum constraints, that is, no-net-rotation and no-net-translation applied on the core stations.

Table 4 presents the average values of the ERP agreement between GNSS and VLBI in CONT05–CONT17, including the improvement of solutions with tropospheric ties compared to the solution without tropospheric ties. The improvements by tropospheric ties are 26, 12, 14, 10, and 5% on the x-pole offset, y-pole offset, x-pole rate, y-pole rate, and LoD, respectively, which are consistent with the improvements when comparing to the IERS EOP 14 C04 product reported earlier. Despite the negative impact of gradient ties on y-pole offset, all other ERP components are improved, especially when both ZTD and gradient ties are applied.

Noticing that the ZTD ties contribute more to the improvement of the PM offsets, whereas the gradient ties contribute more to the PM rates, we further investigated the EOP formal errors, which are presented in Fig. 6. The formal error improvements from ZTD ties on the offsets of x-pole, y-pole, and UT1-UTC are 28, 22, and 15%, respectively, and those on the corresponding rates are 11, 9, and 6%. In comparison, the improvements from gradient ties on the offsets are 21, 19, and 15%, and those on the rates are 17, 17, and 15%. The gradient ties result in larger improvement on the

Table 4 Average WSTD values of the ERP agreement between VLBI and independent GNSS solutions in CONT05–CONT17. The improvement of solutions with respect to the "NO" solution is present in the bracket, where a positive value indicates an improvement

EOP	NO	ZTD	GRD	TRP
x-pole (μas)	90	66 (26%)	80 (11%)	66 (26%)
y-pole (μas)	61	55 (10%)	63 (− 4%)	54 (12%)
x-pole rate (μas/day)	180	160 (10%)	156 (13%)	154 (14%)
y-pole rate (μas/day)	175	172 (2%)	159 (9%)	158 (10%)
LoD (μs/day)	8.8	8.4 (4%)	8.2 (6%)	8.3 (5%)
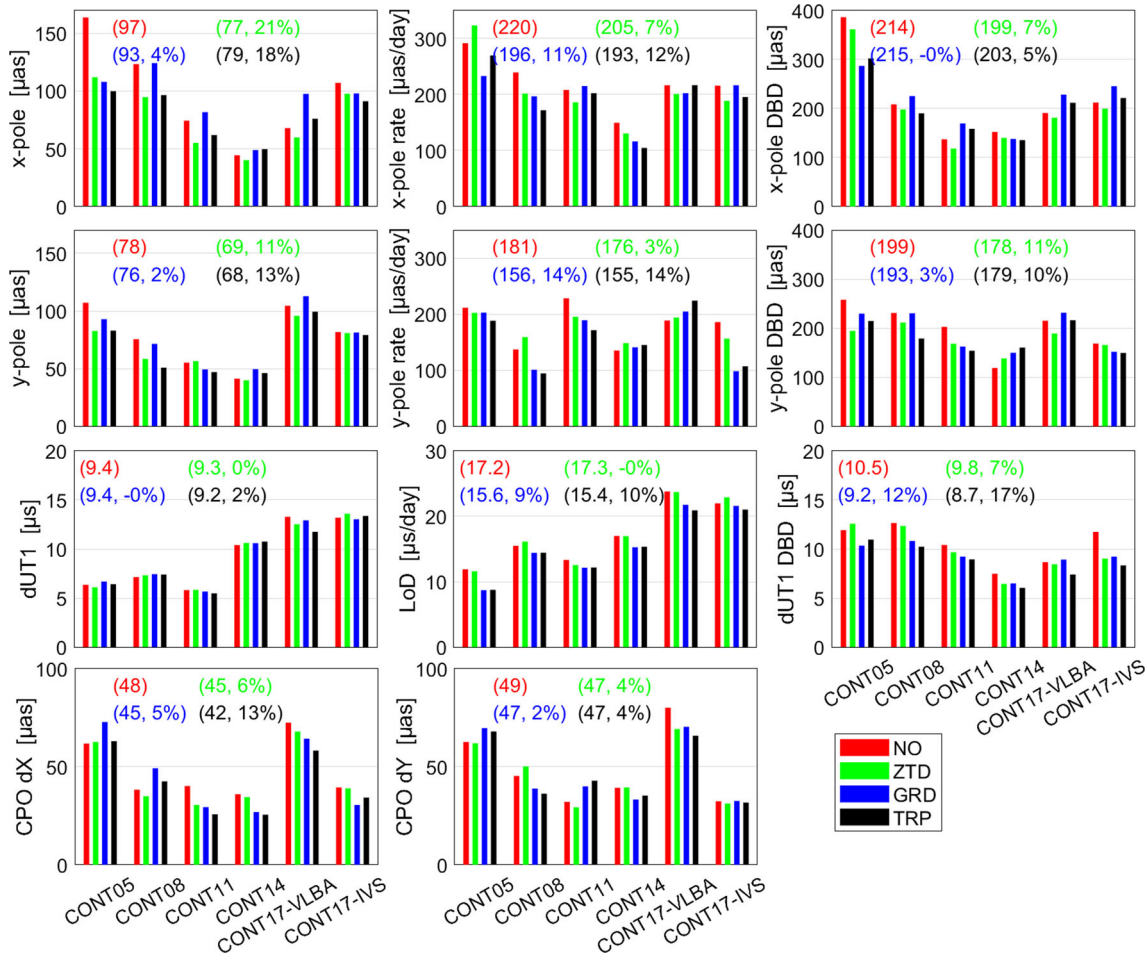
Fig. 5 Left and middle panels: WSTD of the differences between EOP estimated herein and the IERS EOP 14 C04; right panels: WRMS of the polar motion and UT1-UTC day-boundary-discontinuities (DBD). In brackets the average values during CONT05–CONT17 and the improvement of the solutions with tropospheric ties over solutions without tropospheric ties are given

CPO (17%) than the ZTD ties (8–9%). Therefore, the formal errors clearly indicate the different contributions of ZTD and gradient ties on different EOP components.

To better understand the different impacts of ZTD and gradient ties on EOP, Fig. 7 shows the correlation coefficients between the tropospheric parameters and EOP, with and without applying tropospheric ties. We did not consider the tropospheric tie biases in this demonstration because: (1) the correlation coefficient only shows the theoretical situation and is not influenced by the tropospheric tie accuracy, and (2) estimating the tropospheric tie bias introduces correlation between the bias parameter and EOP, which does not exist in the solution without tropospheric ties. Despite the small magnitude of the correlation coefficients, we can see that ERP offsets have a higher correlation with ZTD than gradients, and ERP rates have a higher correlation with gradients (at least one gradient). The CPO (dX and dY) are more

Fig. 6 Average values of EOP formal errors in CONT05–CONT17, with different tropospheric ties applied
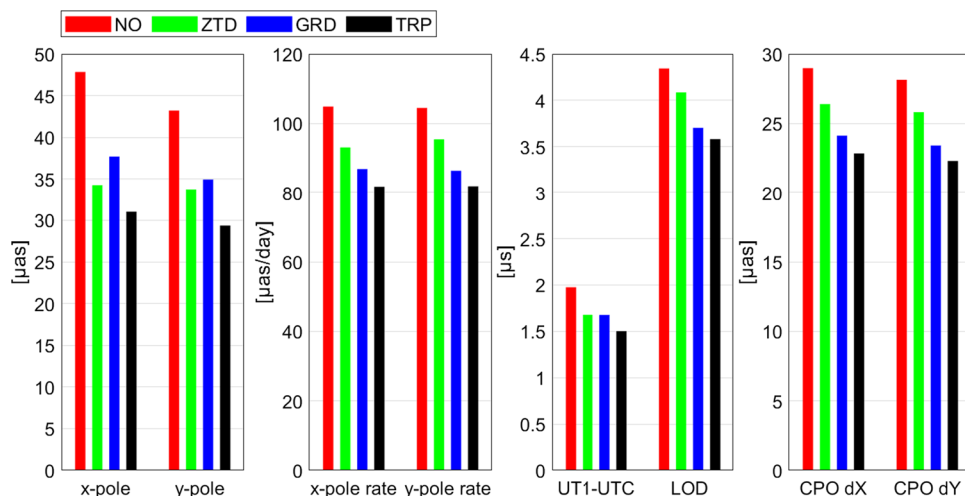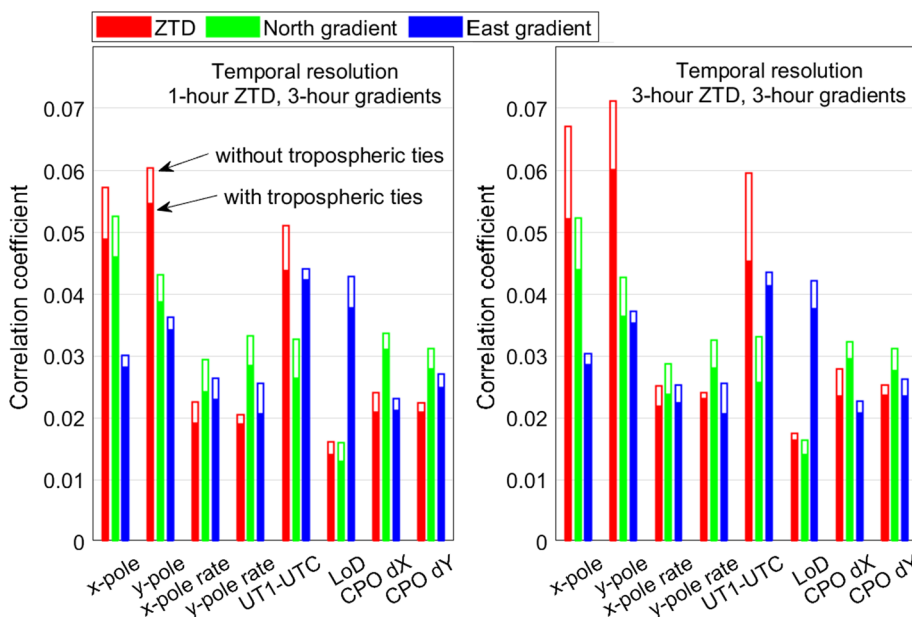

Fig. 7 Correlation coefficients between tropospheric parameters and EOP in session CONT1415 of CONT14. Left: 1-hourly ZTD and 3-hourly gradient resolution; right: 3-hourly ZTD and 3-hourly gradient resolution. The average values of all correlation coefficients in the session over all VLBI stations are presented


correlated with the gradients than with the ZTD. Applying tropospheric ties reduces the correlation, which explains the improvements in EOP formal errors and the agreement to the IERS product. Moreover, we can derive consistent conclusions in the two solutions with different or same temporal resolutions between ZTD and gradients.

Despite the general improvement in most CONT campaigns by applying tropospheric ties, not every campaign shows similar performance. For instance, in CONT17-VLBA the polar motion estimates deteriorate upon applying tropospheric ties (see Fig. 5). This may be caused by assuming the tropospheric tie bias as daily constant, as the different sky coverage between GNSS and VLBI can cause discrepancies. It should be mentioned that the best improvement is usually obtained when both ZTD and gradient ties are applied.

3.3 Tropospheric tie bias

As the a priori tropospheric tie biases from single-technique solutions are used, we further investigate the residual tropospheric tie bias. Figure 8 presents the average values of the residual tropospheric tie bias in CONT11 and CONT14 and the corresponding standard deviation (STD) values. For each co-location, the residual tropospheric tie biases, that is, the tropospheric tie bias estimate minus the a priori value, are averaged over all sessions of the campaign, and the STD value can also be obtained. We can see the residual tropospheric tie biases are usually close to zero with the STD values much larger than the mean values, which is expectable as the a priori bias is derived from the single-technique solution. However, the large STD values indicate that the variation of the bias from session to session cannot be ignored. Moreover, the

Fig. 8 Average values (blue bar) of the residual tropospheric tie bias after subtracting the a priori values and the corresponding standard deviation (red error bar) in CONT11 (left) and CONT14 (right). Upper: ZTD, middle: north gradient, lower: east gradient
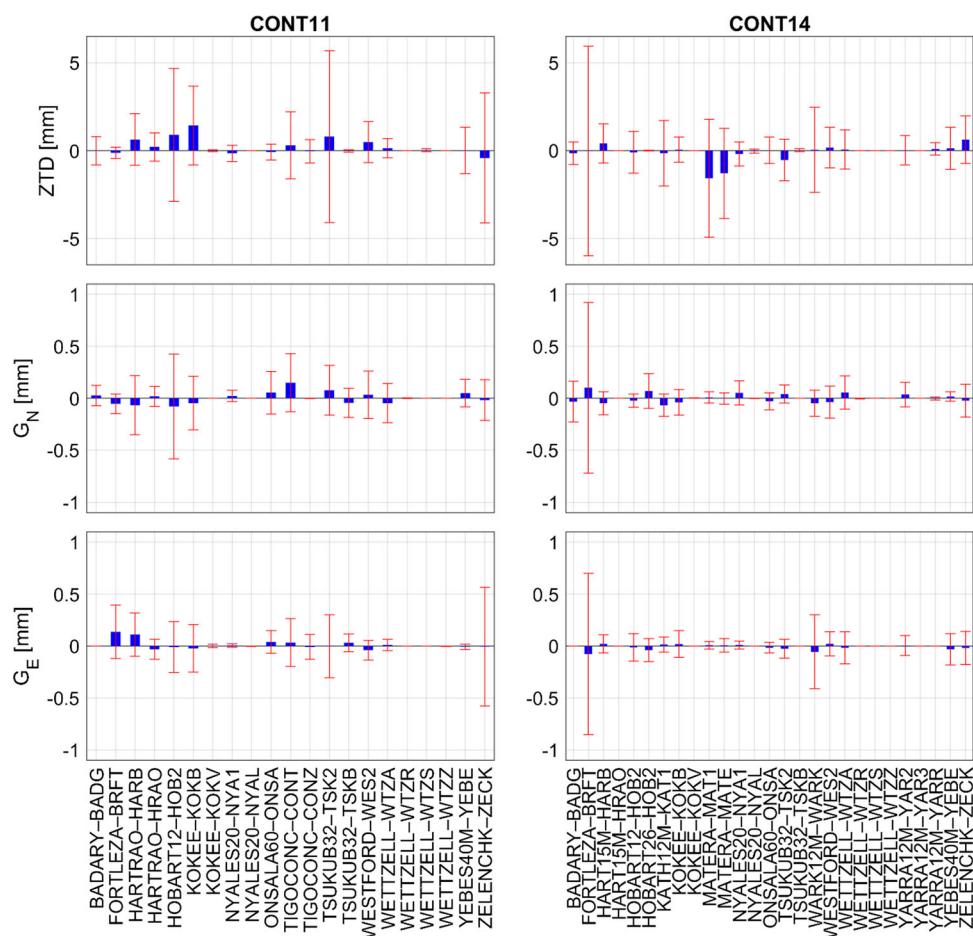
performance of the same co-location may vary significantly between different campaigns. For instance, the FORTLEZA––BRFT co-location has much larger STD values for both ZTD and gradient tie biases in CONT14 than in CONT11, whereas the HOBART12–HOB2, TSUKUBA23–TSK2, and ZELENCHK–ZECK co-locations all have much larger STD values in CONT11 than in CONT14.

4 Summary and conclusions

We demonstrated the benefits of applying tropospheric ties in the VLBI and GNSS integrated processing on the observation level during CONT05–CONT17. We modeled the topography-related tropospheric tie biases using NWM, and proposed an automatic method to handle the instrument-related systematic biases. Applying VLBI–GNSS tropospheric ties improves the observation geometry, especially for VLBI stations, and thus reduces the correlation between tropospheric parameters and station coordinates, hence yielding a stabilized VLBI network and enhanced EOP estimates.

Compared to the solution without tropospheric ties, applying both ZTD and gradient ties improves the VLBI station coordinate repeatability by 12, 12, and 28% in the north, east,

and up components, respectively. The horizontal improvement is mainly from the gradient ties, and the vertical one is mainly from the ZTD ties. The network scale is improved by 32% with the repeatability reduced from 0.60 to 0.40 ppb, mainly due to the ZTD ties.

The VLBI EOP estimates also benefit greatly from tropospheric ties, with the agreements to the IERS EOP product improved by 18, 13, and 2% on x-pole, y-pole, and UT1-UTC components, respectively. The corresponding DBD are improved by 5, 10, and 17%. We demonstrated that the ZTD ties contribute more to the ERP offset improvement, whereas the gradient ties contribute more to the improvement of ERP rates and CPO. This can be illustrated by the correlation coefficients between tropospheric parameters and different EOP components.

Despite the benefits of applying the VLBI–GNSS tropospheric ties, it is worth to mention that the tropospheric parameter agreement between VLBI and GNSS is only about 5 mm for now (Teke et al. 2011, 2013), which may cause slight deterioration in EOP estimates upon applying tropospheric ties. In addition, the tropospheric tie biases that are not related to topography should be further investigated. The VLBI and GNSS combination using additional global ties

and local ties (Glaser et al. 2018) was investigated (Wang 2021).

This study is an important step toward the multi-technique integrated processing on the observation level to include all available ties, especially the tropospheric ties for the microwave-based techniques. In further ITRF determination, especially the epoch-specific ITRF (Bloßfeld et al. 2013; Abbondanza et al. 2017), the tropospheric ties can contribute greatly to improve the network stability, especially the scale parameter. The VLBI EOP estimates improved by the tropospheric ties indicate the advantage to apply tropospheric ties in future VLBI processing, especially considering that the VLBI is the only technique capable of determining UT1-UTC and CPO. The enhanced EOP product from IVS can better serve the monitoring of the Earth dynamic system.

References

Abbaszadeh M, Clarke PJ, Penna NT (2020) Benefits of combining GPS and GLONASS for measuring ocean tide loading displacement. J Geod. https://doi.org/10.1007/s00190-020-01393-5

Abbondanza C, Chin TM, Gross RS, Heflin MB, Parker JW, Soja BS, van Dam T, Wu X (2017) JTRF2014, the JPL Kalman filter and smoother realization of the International Terrestrial Reference System. J Geophys Res Solid Earth 122:8474–8510. https://doi.org/10.1002/2017jb014360

Altamimi Z, Rebischung P, Métivier L, Collilieux X (2016) ITRF2014: a new release of the International Terrestrial Reference Frame modeling nonlinear station motions. J Geophys Res Solid Earth 121:6109–6131. https://doi.org/10.1002/2016jb013098

Baarda W (1968) A testing procedure for use in geodetic network. Publ Geod 9:2

Behrend D, Thomas C, Gipson J, Himwich E, Le Bail K (2020) On the organization of CONT17. J Geod. https://doi.org/10.1007/s00190-020-01436-x

Bender M, Dick G, Wickert J, Schmidt T, Song S, Gendt G, Ge M, Rothacher M (2008) Validation of GPS slant delays using water vapour radiometers and weather models. Meteorol Z 17:807–812. https://doi.org/10.1127/0941-2948/2008/0341

Bizouard C, Lambert S, Gattano C, Becker O, Richard J-Y (2018) The IERS EOP 14C04 solution for Earth orientation parameters consistent with ITRF 2014. J Geod 93:621–633. https://doi.org/10.1007/s00190-018-1186-3

Bloßfeld M, Seitz M, Angermann D (2013) Non-linear station motions in epoch and multi-year reference frames. J Geod 88:45–63. https://doi.org/10.1007/s00190-013-0668-6

Böhm J, Schuh H (2013) Atmospheric effects in space geodesy. Springer-Verlag, Berlin Heidelberg

Charlot P, Jacobs CS, Gordon D, Lambert S, de Witt A, Böhm J, Fey AL, Heinkelmann R, Skurikhina E, Titov O, Arias EF, Bolotin S, Bourda G, Ma C, Malkin Z, Nothnagel A, Mayer D, MacMillan DS, Nilsson T, Gaume R (2020) The third realization of the International Celestial Reference Frame by very long baseline interferometry. Astron Astrophys 644:A159. https://doi.org/10.1051/0004-6361/202038368

Chen G, Herring TA (1997) Effects of atmospheric azimuthal asymmetry on the analysis of space geodetic data. J Geophys Res Solid Earth 102:20489–20502. https://doi.org/10.1029/97jb01739

Diamantidis P-K, Kłopotek G, Haas R (2021) VLBI and GPS inter- and intra-technique combinations on the observation level for evaluation of TRF and EOP. Earth Planets Space. https://doi.org/10.1186/s40623-021-01389-1

Eriksson D, MacMillan DS, Gipson JM (2014) Tropospheric delay ray tracing applied in VLBI analysis. J Geophys Res Solid Earth 119:9156–9170. https://doi.org/10.1002/2014jb011552

Fernandes MJ, Lázaro C, Ablain M, Pires N (2015) Improved wet path delays for all ESA and reference altimetric missions. Remote Sens Environ 169:50–74. https://doi.org/10.1016/j.rse.2015.07.023

Glaser S, Fritsche M, Sośnica K, Rodríguez-Solano CJ, Wang K, Dach R, Hugentobler U, Rothacher M, Dietrich R (2015) A consistent combination of GNSS and SLR with minimum constraints. J Geod 89:1165–1180. https://doi.org/10.1007/s00190-015-0842-0

Glaser S, König R, Neumayer KH, Nilsson T, Heinkelmann R, Flechtner F, Schuh H (2018) On the impact of local ties on the datum realization of global terrestrial reference frames. J Geod 93:655–667. https://doi.org/10.1007/s00190-018-1189-0

Glaser S, Michalak G, König R, Männel B, Schuh H (2020) Future GNSS infrastructure for improved geodetic reference frames. In: 2020 European navigation conference (ENC), Dresden, Germany, pp 1–10. https://doi.org/10.23919/ENC48637.2020.9317460

Griffiths J (2018) Combined orbits and clocks from IGS second reprocessing. J Geod. https://doi.org/10.1007/s00190-018-1149-8

Heinkelmann R, Willis P, Deng Z, Dick G, Nilsson T, Soja B, Zus F, Wickert J, Schuh H (2016) Multi-technique comparison of atmospheric parameters at the DORIS co-location sites during CONT14. Adv Space Res 58:2758–2773. https://doi.org/10.1016/j.asr.2016.09.023

Hobiger T, Otsubo T (2014) Combination of GPS and VLBI on the observation level during CONT11—common parameters, ties and inter-technique biases. J Geod 88:1017–1028. https://doi.org/10.1007/s00190-014-0740-x

Hobiger T, Shimada S, Shimizu S, Ichikawa R, Koyama Y, Kondo T (2010) Improving GPS positioning estimates during extreme weather situations by the help of fine-mesh numerical weather models. J Atmos Solar Terr Phys 72:262–270. https://doi.org/10.1016/j.jastp.2009.11.018

Hofmeister A, Böhm J (2017) Application of ray-traced tropospheric slant delays to geodetic VLBI analysis. J Geod 91:945–964. https://doi.org/10.1007/s00190-017-1000-7

Huang W, Männel B, Sakic P, Ge M, Schuh H (2020) Integrated processing of ground- and space-based GPS observations: improving GPS satellite orbits observed with sparse ground networks. J Geod. https://doi.org/10.1007/s00190-020-01424-1

Johnston G, Riddell A, Hausler G (2017) The international GNSS service. In: Teunissen PJG, Montenbruck O (eds) Springer handbook of global navigation satellite systems, 1st edn. Springer International Publishing, Cham, Switzerland, pp 967–982. https://doi.org/10.1007/978-3-319-42928-1_33

Kouba J (2007) Implementation and testing of the gridded Vienna Mapping Function 1 (VMF1). J Geod 82:193–205. https://doi.org/10.1007/s00190-007-0170-0

Krügel M, Thaller D, Tesmer V, Rothacher M, Angermann D, Schmid R (2007) Tropospheric parameters: combination studies based on homogeneous VLBI and GPS data. J Geod 81:515–527. https://doi.org/10.1007/s00190-006-0127-8

Kuehn CE, Himwich WE, Clark TA, Ma C (1991) An evaluation of water vapor radiometer data for calibration of the wet path delay in very long baseline interferometry experiments. Radio Sci 26:1381–1391. https://doi.org/10.1029/91rs02020

Landskron D, Böhm J (2017) VMF3/GPT3: refined discrete and empirical troposphere mapping functions. J Geod 92:349–360. https://doi.org/10.1007/s00190-017-1066-2

Landskron D, Böhm J (2018) Refined discrete and empirical horizontal gradients in VLBI analysis. J Geod. https://doi.org/10.1007/s00190-018-1127-1

Lehmann R (2012) Improved critical values for extreme normalized and studentized residuals in Gauss–Markov models. J Geod 86:1137–1146. https://doi.org/10.1007/s00190-012-0569-0

Liu J, Ge M (2003) PANDA software and its preliminary result of positioning and orbit determination. Wuhan Univ J Nat Sci 8:603–609. https://doi.org/10.1007/BF02899825

Liu Y, Ge M, Shi C, Lou Y, Wickert J, Schuh H (2016) Improving integer ambiguity resolution for GLONASS precise orbit determination. J Geod 90:715–726. https://doi.org/10.1007/s00190-016-0904-y

Männel B, Dobslaw H, Dill R, Glaser S, Balidakis K, Thomas M, Schuh H (2019) Correcting surface loading at the observation level: impact on global GNSS and VLBI station networks. J Geod 93:2003–2017. https://doi.org/10.1007/s00190-019-01298-y

Nilsson T, Soja B, Balidakis K, Karbon M, Heinkelmann R, Deng Z, Schuh H (2017a) Improving the modeling of the atmospheric delay in the data analysis of the Intensive VLBI sessions and the impact on the UT1 estimates. J Geod 91:857–866. https://doi.org/10.1007/s00190-016-0985-7

Nilsson T, Soja B, Karbon M, Heinkelmann R, Schuh H (2017b) Water vapor radiometer data in very long baseline interferometry data analysis. In: Freymueller JT, Sánchez L (eds) International symposium on earth and environmental sciences for future generations. International Association of Geodesy Symposia, vol 147. Springer, Cham. https://doi.org/10.1007/1345_2017_264

Noll CE (2010) The crustal dynamics data information system: a resource to support scientific analysis using space geodesy. Adv Space Res 45:1421–1440. https://doi.org/10.1016/j.asr.2010.01.018

Penna NT, Morales Maqueda MA, Martin I, Guo J, Foden PR (2018) Sea surface height measurement using a GNSS wave glider. Geophys Res Lett 45:5609–5616. https://doi.org/10.1029/2018gl077950

Petit G, Luzum B, IERS conventions (2010) (IERS Technical Note No. 36). In: Frankfurt am Main

Pollet A, Coulot D, Bock O, Nahmani S (2014) Comparison of individual and combined zenith tropospheric delay estimations during CONT08 campaign. J Geod 88:1095–1112. https://doi.org/10.1007/s00190-014-0745-5

Rebischung P, Schmid R (2016) IGS14/igs14.atx: a new framework for the IGS products. In: AGU Fall Meeting 2016. https://mediatum.ub.tum.de/doc/1341338/file.pdf

Shamshiri R, Motagh M, Nahavandchi H, Haghshenas Haghighi M, Hoseini M (2020) Improving tropospheric corrections on large-scale Sentinel-1 interferograms using a machine learning approach for integration with GNSS-derived zenith total delay (ZTD). Remote Sens Environ 239:111608. https://doi.org/10.1016/j.rse.2019.111608

Steigenberger P, Tesmer V, Krügel M, Thaller D, Schmid R, Vey S, Rothacher M (2007) Comparisons of homogeneously reprocessed GPS and VLBI long time-series of troposphere zenith delays and gradients. J Geod 81:503–514. https://doi.org/10.1007/s00190-006-0124-y

Teke K, Böhm J, Nilsson T, Schuh H, Steigenberger P, Dach R, Heinkelmann R, Willis P, Haas R, García-Espada S, Hobiger T, Ichikawa R, Shimizu S (2011) Multi-technique comparison of troposphere zenith delays and gradients during CONT08. J Geod 85:395–413. https://doi.org/10.1007/s00190-010-0434-y

Teke K, Nilsson T, Böhm J, Hobiger T, Steigenberger P, García-Espada S, Haas R, Willis P (2013) Troposphere delays from space geodetic techniques, water vapor radiometers, and numerical weather models over a series of continuous VLBI campaigns. J Geod 87:981–1001. https://doi.org/10.1007/s00190-013-0662-z

Teke K, Böhm J, Madzak M, Kwak Y, Steigenberger P (2015) GNSS zenith delays and gradients in the analysis of VLBI Intensive sessions. Adv Space Res 56:1667–1676. https://doi.org/10.1016/j.asr.2015.07.032

Thaller D, Krügel M, Rothacher M, Tesmer V, Schmid R, Angermann D (2006) Combined Earth orientation parameters based on homogeneous and continuous VLBI and GPS data. J Geod 81:529–541. https://doi.org/10.1007/s00190-006-0115-z

Wang J (2021) Integrated Processing of GNSS and VLBI on the observation level. PhD Thesis, Technische Universität Berlin. https://doi.org/10.14279/depositonce-12513

Wang J, Liu Z (2019) Improving GNSS PPP accuracy through WVR PWV augmentation. J Geod 93:1685–1705. https://doi.org/10.1007/s00190-019-01278-2

Wang J, Wu Z, Semmling M, Zus F, Gerland S, Ramatschi M, Ge M, Wickert J, Schuh H (2019) Retrieving precipitable water vapor from shipborne multi-GNSS observations. Geophys Res Lett 46:5000–5008. https://doi.org/10.1029/2019gl082136

Wijaya DD, Böhm J, Karbon M, Kràsnà H, Schuh H (2013) Atmospheric pressure loading. In: Böhm J, Schuh H (eds) Atmospheric effects in space geodesy. Springer, Berlin, Heidelberg, pp 137–157. https://doi.org/10.1007/978-3-642-36932-2_4

Williams S, Bock Y, Fang P (1998) Integrated satellite interferometry: tropospheric noise, GPS estimates and implications for interferometric synthetic aperture radar products. J Geophys Res Solid Earth 103:27051–27067. https://doi.org/10.1029/98jb02794

Wu JT, Wu SC, Hajj GA, Bertiger WI, Lichten SM (1993) Effects of antenna orientation on GPS carrier phase. Manuscripta Geodaet 18:91–98

Wu Z, Liu Y, Liu Y, Wang J, He X, Xu W, Ge M, Schuh H (2020) Validating HY-2A CMR precipitable water vapor using ground-based and shipborne GNSS observations. Atmos Meas Tech 13:4963–4972. https://doi.org/10.5194/amt-13-4963-2020

Zumberge JF, Heflin MB, Jefferson DC, Watkins MM, Webb FH (1997) Precise point positioning for the efficient and robust analysis of GPS data from large networks. J Geophys Res Solid Earth 102:5005–5017. https://doi.org/10.1029/96jb03860